Shelling the Voronoi interface of protein-protein complexes predicts residue activity and conservation

Benjamin Bouvier [a,c,]* Raik Grünberg [b,]* Michael Nilges [c]

Frederic Cazals [a,]**

[a]*INRIA Sophia-Antipolis, Project Geometrica, F-06902 Sophia-Antipolis, France*

[b]*EMBL-CRG Systems Biology Unit, CRG–Centre de Regulacio Genomica, Dr. Aiguader 88, 08003 Barcelona, Spain*

[c]*Unit de Bioinformatique Structurale, Institute Pasteur, 75724 Paris Cedex 15, France*

Abstract

The accurate description of protein-protein interfaces remains a challenging task. Traditional criteria, based on atomic contacts or changes in solvent accessibility, tend to over or underpredict the interface itself and cannot discriminate active from less relevant parts. A recent molecular dynamics simulation study by Mihalek and co-authors concluded that active residues tend to be 'dry', that is, insulated from water fluctuations. We show that patterns of 'dry' residues can, to a large extent, be predicted by a fast, parameter-free and purely geometric analysis of protein interfaces. We introduce the shelling order of Voronoi facets as a straightforward quantitative measure of an atom's depth inside an interface. We analyze the correlation between Voronoi shelling order, dryness, and conservation on a set of 54 protein-protein complexes. Residues with high shelling order tend to be dry; evolutionary conservation also correlates with dryness and shelling order but, perhaps not surprisingly, is a much less accurate predictor of either property. Voronoi shelling order thus seems a meaningful and efficient descriptor of protein interfaces. Moreover, the strong correlation with dryness suggests that water dynamics within protein interfaces may, in first approximation, be described by simple diffusion models.

Key words:

Protein-protein complex, interface activity, hotspots, conservation, Voronoi models.

PACS:

* both authors contributed equally

**Corresponding author

Email address: Frederic.Cazals@sophia.inria.fr (Frederic Cazals).

1 INTRODUCTION

Specific recognition between proteins plays a crucial role in almost all cellular processes and most proteins are embedded in highly connected (and dynamically changing) networks of interaction partners [1]. Despite much progress [2], identifying the exact interface between two proteins remains difficult. On the one hand, exact predictions are hindered by the complex and dynamic nature of proteins [3,4]; on the other hand, the descriptors we employ to study the interface may be flawed or ill-chosen.

A protein-protein interface is traditionally defined by the 'geometric footprint', which refers to all atoms within a given distance of the interaction partner. Somewhat more precise definitions rely on the loss of solvent accessibility (SA) upon binding [5]. Yet, as much as half of this footprint can seemingly be irrelevant to binding [6]. As contributions to specificity and affinity appeared very unevenly distributed, substantial effort has been spent on the identification of areas or residue patches that are actively involved in molecular recognition [7–10]. This lead to the definition of 'hotspot' residues [11,12]. Hotspots refer to the usually very small number [12] of 'key' residues in a protein-protein interface, the mutation of which causes large changes in the binding free energy. Contrary to this focus on isolated residues, more recent studies have revealed strong non-additive, collective effects [13] which point to a modular organization of interfaces into interaction clusters [14].

Also the evolutionary record seems of limited use for distinguishing relevant from irrelevant. The sequence conservation of protein-protein interfaces is hardly statistically significant and depends heavily on surface-patch selection

3

25 techniques [15]. A commonly adopted view states that, unlike catalytic sites

26 that are highly unlikely to transform in a series of discrete steps without com-

27 plete loss of activity [16], the assembly of proteins involves a continuous scale

28 of binding modes, from transient to stable, leaving more freedom for evolution

29 to proceed in incremental steps [17–19]. Interestingly, conservation signals be-

30 come more convincing if one turns away from individual– and towards patches

31 [20] or clusters of residues [21].

32 Water forms an essential part of protein-protein interfaces [9,22]. The occlusion

33 of bulk solvent is a common denominator not only of classical hotspots [23],

34 but also of the more recently identified interaction modules [14], which are

35 delimited by structural water. In fact, the removal of water from partially

36 solvated backbone hydrogen bonds has been argued to be a driving force of

37 binding [24,25].

38 Recently, Mihalek and coworkers [26] went one step further and classified inter-

39 face residues by the dynamics of surrounding water molecules. They asserted

40 that the important residues are the ones whose interactions are not disturbed

41 by water fluxes. These 'dry' residues (some of which may actually be in con-

42 tact with immobile, structural water molecules) were found to correlate better

43 with conservation than the overall geometric footprint and to feature some

44 characteristic properties of classical hotspots. The dryness results collated by

45 these authors on a variety of systems thus represent valuable information as

46 a measure of residue importance; we will constantly refer to them during this

47 work.

48 However, the method suffers from some drawbacks. It relies on molecular dy-

49 namics simulations which are computationally expensive and sensitive to setup

4

50 and parameterization. Furthermore, it cannot itself distinguish between inter-

51 face and noninterface residues. Mihalek and coworkers addressed this problem

52 by discarding residues that are also dry in the isolated partners, hereby further

53 increasing computational costs and neglecting the possibility of conformational

54 transitions upon binding.

55 All in all, the combination of the large size of protein-protein interfaces, the

56 relatively small areas that appear actually important and the lack of unam-

57 biguous ways to identify them, amounts to a difficult problem for which novel

58 approaches are highly desirable. We present a method based on the shelling

59 of the Voronoi interface of protein-protein complexes. The method quantifies

60 the depth of any given atom inside the interface, in a manner accounting for

61 both the geometry and the topology of the interface. The method is simulta-

62 neously accurate, computationally inexpensive, and elegant in that it does not

63 require parameterization. Voronoi shelling order features an excellent correla-

64 tion with the water shielding observed by Mihalek et al., without the need for

65 simulations or geometric footprinting. We analyze the relationship between

66 three quantities of interest (Voronoi shelling order, dryness and conservation)

67 on the same set of protein complexes. We illustrate the advantages as well as

68 potential improvements of the geometric measure with detailed examples and

69 elaborate on the more complex correlation with evolutionary information.

2 THEORY

2.1 Voronoi description of protein-protein interfaces

In this section, we briefly summarize the Voronoi model of protein-protein interfaces, which is described in more detail in [27], together with a comprehensive bibliography. Given a collection of sample points equipped with the Euclidean distance, the Voronoi diagram is the space partition which assigns to every sample the convex polyhedron containing all points in space closer to it than to any other sample. In 3D space, these Voronoi regions are bounded by Voronoi facets (resp. edges, vertices) which consist of points equidistant from two (resp. three, four) samples.

The Euclidean Voronoi diagram of atom centers in a molecule, first employed by Richards [28] to investigate packing properties in proteins, is unable to account for the fact that different atoms have different radii. A convenient generalization thereof, which overcomes this limitation while retaining non-curved bisectors, is the power diagram[29]. It replaces the Euclidean distance with the 'power distance' of a point to a sphere centered at $\mathbf{a}$ and of radius r: $p(\mathbf{x}) = |\mathbf{a} - \mathbf{x}|^2 - r^2$. The power diagram is an extension of the Voronoi diagram (to which it reverts for atoms of equal radii); hence, we continue to refer to it as such in the text. Throughout the study, we compute it for atomic spheres whose radii are the so-called group radii [30], expanded by the radius of a probe water molecule $r_w = 1.4$ Å. This effectively models the solvent-accessible surface (SAS) of the protein, as defined by Lee and Richards [31]. An example Voronoi diagram for a hypothetical two-dimensional molecule is shown on Figure 1.

6

94 The Voronoi diagram has a dual (an associated and strictly equivalent struc-

95 ture) called the Delaunay triangulation; in practice, Voronoi diagrams are

96 calculated via their Delaunay triangulation rather than directly. The Delau-

97 nay triangulation consists of edges (resp. triangles, tetrahedra) that connect

98 the centers of two (resp. three, four) adjacent spheres whose corresponding

99 Voronoi regions share a facet (resp. an edge, a vertex).

100 When modeling molecules, a drawback of the Voronoi diagram is that atoms

101 located on the convex hull have unbounded Voronoi regions (all but the region

102 of atom a_2, on Figure 1). An elegant way of solving this problem is to use

103 a restriction of the Delaunay triangulation called the α-complex [32]. For a

104 fixed value of α, each ball of center $\mathbf{a_i}$ and radius r_i is replaced by a ball of

105 center $\mathbf{a_i}$ and radius $\sqrt{r_i^2 + \alpha}$. Given these expanded balls, the construction

106 of the α-complex mimics that of the Delaunay triangulation, to the extent

107 that one focuses on the intersection of the restriction of each expanded ball

108 to its Voronoi region rather than the Voronoi region itself; see Figure 1 for an

109 illustration. Varying the value of α allows for the investigation of properties

110 at different scales. In particular, for very large values of α the α-complex

111 is identical to the Delaunay triangulation. In rare occurrences of desolvated

112 models, an additional filtering step may be necessary to discard all instances

113 of unphysically large facets at the rim of the interface [27]; we do not discuss

114 this issue further since this study involves solvated models only.

115 We now apply this methodology to model the interface between two proteins

116 A and B. Following [27], the AB interface consists of the Delaunay edges

117 found in the 0-complex – the α-complex for $\alpha = 0$, and whose endpoints

118 belong to A and B. Because of the duality between the Delaunay and Voronoi

119 representations, the interface can also be described using the Voronoi facets

7

120 dual to the aforementioned edges. The interface model can be extended to

121 accommodate interface water molecules W, defined as sharing at least one

122 edge with each partner in the 0-complex. This allows for the definition of

123 the following interfaces: AB between the protein partners; AW (resp. BW)

124 between partner A (resp. B) and interface water; $AW-BW$ as the union of the

125 interfaces AW and BW; ABW as the union of the interfaces AB and $AW-$

126 BW. Like other methods mentioned above, our model correctly identifies any

127 atom losing solvent accessibility as an interface atom. Unlike these methods

128 however, it also detects interface atoms that do not lose solvent accessibility

129 – essentially buried backbone atoms, these represent a non-negligible 13% of

130 the interface [27].

131 *2.2   Shelling the ABW interface*

132 The next step of the algorithm attributes a Voronoi shelling order (VSO)

133 to each facet of the ABW interface. This represents the number of 'jumps'

134 between adjacent facets that needs to be performed, from the currently con-

135 sidered location, to reach the rim of the interface (Figures 2a and 3a). The

136 Voronoi interface is thus partitioned into concentric shells of increasing selling

137 order.

138 The calculation of VSO values for all interface facets requires two passes.

139 During the first pass, boundary Voronoi facets located at the rim of the in-

140 terface are enumerated and given a VSO of one. Voronoi facets are bounded

141 by Voronoi edges, each of which is incident to exactly three Voronoi facets

142 in the Voronoi diagram; however, some of these facets may not belong to the

143 interface (their dual Delaunay edges are not in the 0-complex). This allows us

8

144   to detect rim Voronoi facets as the ones featuring at least one Voronoi edge

145   that is incident to one interface Voronoi facet only. The second pass explores

146   the interface breadth-first starting from the previously identified rim facets.

147   Given an interface Delaunay edge (of shelling order n), the algorithm checks

148   all incident Delaunay triangles, as each such triangle contributes zero, one or

149   two additional interface edges. If these have not already been shelled, they are

150   given a VSO of $n + 1$. To speed up the search operations, a temporary map

151   storing edges of VSO $n - 1$, n and $n + 1$ is used, since these are the only ones

152   that can be encountered at level n; the contents of this map are copied over

153   to a permanent structure each time n increases.

154   The outcome of this process is the association of an integer VSO value to

155   each Delaunay edge (or equivalently, Voronoi facet) of the ABW interface.

156   However, our ultimate goal is to quantify the depth of any given atom in-

157   side the interface. This is done by tagging the atom with the minimum value

158   among the shelling orders of the Delaunay edges to which the atom contributes

159   (Figures 2b and 3b). The maximum or average values have also been consid-

160   ered as candidates, but their variation throughout the interface were found to

161   closely mimic that of the minimum. Finally, the shelling order of a residue,

162   defined as the average VSO value over its constituent atoms contributing to

163   the Voronoi interface, is employed when comparing to residue-based measures

164   such as conservation or dryness.

9

3 RESULTS

3.1 Voronoi shelling order, conservation and water dynamics

A recent simulation study examined the rate at which residues in protein-protein interfaces exchange surrounding water molecules [26]. Residues that were mostly shielded from mobile water molecules, defined as "dry" by Mihalek et al., turned out to be more conserved and were thus interpreted as the active part of the interface. Our initial goal is to assess how well shelling order is able to predict dryness on the set of homo- and heterodimer complexes studied by Mihalek et al. [26]. As a yardstick, we compare to the previously established correlation between conservation and dryness. Conservation is determined from pFam [33] hidden Markov models [34] using a relative entropy scheme [35]. In order to characterize all possible relationships, we also examine, further down in the text, how good a predictor of shelling order conservation is. We generate three ROC plots for each complex, describing the performance of shelling order as predictor of dryness, of conservation as predictor of dryness and of conservation as predictor of shelling order, respectively. A representative example set of ROC curves is shown in Figure 4. The area between each ROC curve and the diagonal quantifies the predictive power of a score (i.e. VSO, conservation) in terms of sensitivity and specificity. An area of 0.5 corresponds to a perfect prediction, which in the example of shelling order predicting dryness means that the n dry residues in the interface perfectly match the n residues with highest shelling order without any over-prediction. By contrast, a ROC area of 0 corresponds to the performance of a pure random classifier. See Section 5.4 for details.

10

The results are compiled in Tables 1 and 2 for heterodimers and homodimers, respectively, and summarized in Figure 5. Evidently, Voronoi shelling order is a very good predictor of dryness and outperforms conservation for 35 of the 36 homodimers and 17 of the 18 heterodimers. VSO always performs better than a purely random classifier, whereas conservation fails to do so in seven cases (five homodimers and two heterodimers). The third columns of Tables 1 and 2 quantify the ability of sequence conservation to predict Voronoi shelling order. We define the n_{core} residues with highest VSO as 'core' and the remainder as 'rim' and test the ability of conservation to discriminate between the two. We adjust n_{core} for each complex so as to exactly match the number of residues classified as dry. We thus tie ourselves to a threshold chosen by Mihalek et al. [26] rather than optimizing our own. Nevertheless, the connection from conservation to Voronoi shelling order appears as good as it is to dryness. While the results differ in detail, the average ROC area is 0.15 for heterodimers and 0.12 for homodimers, which compares well with the respective figures of 0.14 and 0.13 for the prediction of water shielding. However, both conservation-based predictions are outperformed by the much closer correlation between shelling order and dryness, reflected by average ROC areas of 0.31 and 0.34. This notable discrepancy indicates a more direct link between the two latter properties, both of which are structure-based.

3.2 Spatial distribution of conserved residues

The analysis of the ROC curves provides insight into the location of highly conserved residues across the interface shells: conservation becomes a mediocre predictor for Voronoi shelling order when highly conserved residues are found

11

213 at low VSO (such residues are expected to be wet) and/or when poorly con-

214 served residues are found at high VSO (such residues are expected to be dry).

215 However, this simplified focus on extreme values can not fully capture the

216 spatial distribution of conservation. We therefore now address two comple-

217 mentary points, namely (i) the average residue conservation as a function of

VSO, and (ii) the cumulated conservation score over consecutive shells.

218

219 (i) Guharoy and Chakrabarti showed that residues at the interface core are,

220 on average, more conserved than those on the rim [36]. Their binary interface

221 model defined the rim as all residues that are not fully buried inside the com-

222 plex. Our more quantitative description helps to refine the prior conclusion.

223 We normalize conservation scores and Voronoi shelling order so that both span

224 the range 0 to 1 for each interface. We then compute the average conserva-

225 tion score as a function of VSO using a large moving window comprising 1/4

226 of all interface residues. Figures 6 and 7 show this running average for all

227 complexes. The relation between residue conservation on the one hand, and

228 depth within the interface on the other, is evidently not a simple one. The

229 non-averaged original values (gray lines) highlight the scattering of conserva-

230 tion across shells: highly conserved residues are found even at the very rim.

231 Only the extensive averaging reveals a clear correlation between increases in

232 shelling order and residue conservation. This observation is not sensitive to

233 the actual averaging window and the curves remain very similar for window

234 sizes between 1/8 and 1/2 of the interface (data not shown).

235 The overall correlation between shelling order and conservation can be quan-

236 tified in a single number by double integration over the running average. We

237 denote $c(x)$ the average conservation score at $VSO = x$ and reset the baseline

12

238   of this function to 0 by substracting the minimum value m: $\overline{c}(x) = c(x) - m$.

239   We now define $A = \int_0^1 \overline{c}(t)dt$ to be the area under this running average and we

240   normalize $\overline{c}(x)$ to cover an area of 1: $f(x) = (c(x) - m)/A$. Function $f(x)$ can be

241   seen as a probability density function, with associated cumulated distribution

242   function $F(x) = \int_0^x f(t)dt$ (dash-dotted line in figures 6 and 7). One always has

243   $F(1) = 1$, but the speed at which F reaches 1 depends on whether conserved

244   residues are picked up early (in the outer shells) or late (inner shells). F thus

245   encodes the cumulative conservation score up to shelling order x. To provide

246   a concise measure of this property, we report $g(x) = \int_0^x F(t)dt$ (dotted line in

247   figures 6 and 7). The total area under F depends on the overall distribution of

248   conservation across shells. Lower values of $g(1)$ thus indicate that conserved

249   residues tend to cluster towards the *core* of the interface; values above 0.5 (the

250   double integral over a flat line) denote clustering near the *rim*. The deviation

251   $\Delta = g(1) - 0.5$ is reported in the lower right corner of each plot in figures

252   6 and 7. $g(1)$ falls below a value of 0.5 for 15 out of 18 heterodimers and

253   28 out of 36 homodimers. Conservation thus generally increases towards the

254   interface core. Nevertheless, apart from the few obvious exceptions, closer in-

255   spection also reveals some interesting systematic deviations: (i) Conservation

256   density often reaches its maximum before the innermost shell – the interface

257   center thus appears under less constraint than a surrounding outer core; (ii)

258   contrary to the overall trend, a pronounced secondary peak of conservation is

259   sometimes apparent at the very edge of the interface.

260   (ii) While the previous analysis focuses on the spatial distribution of conser-

261   vation per se, it is also worthwhile to compare the spatial distribution of con-

262   servation for two sets of residues: the interface residues and the dry residues.

263   The detailed analysis is described in section A.1 of the supplemental material.

13

264 Non-interface residues account for a proportion of the total conservation score

265 (over the whole protein) in the range 60% to 84% in heterodimers (average

266 76%), and 36% to 97% for homodimers (average 73%) –see the second column

267 of Tables A.1 and A.2 in the supplemental material. These results alone show

268 that the effect of the majority of conserved residues on the interface is at best

269 an indirect one –for example, through the imposition of a protein fold which in

270 turn dictates interface structure. Moreover, the comparison of the area under

271 the cumulated distribution function for interfacial and dry residues performed

272 in Section A.1 confirms that the rim amino-acids account for a non-negligible

273 part of the conservation. The good agreement with the scattered conservation

274 signals and conserved interface rims observed in figures 6 and 7 allows us to

275 rule out a purely statistical effect where a large number of moderately con-

276 served rim residues might end up having more weight than a small number

277 of highly conserved core amino-acids: highly conserved residues do occur on a

278 non fortuitous basis at the rim of protein-protein interfaces.

279 The in-depth examination of average and cumulated conservation thus con-

280 firms the general trend of higher conservation towards core shells but also

281 hints at a more complex fine structure. The very center of an interface often

282 appears more amenable to change than its immediate surroundings; further-

283 more, numerous interfaces seem to bear substantial evolutionary pressure on

284 their outer rims. From the inspection of examples, we speculate this latter

285 signal to be a signature of electrostatic steering [37] but the issue deserves

286 further scrutiny.

14

287 *3.3 Case-studies: best and worst case scenarios for shelling order*

288 To identify in more detail the incentives and shortcomings of using shelling

289 order for the description of interfaces and as a predictor of water dynamics, we

290 focus on three extreme cases of application, which are presented in Figure 8.

291 *The ideal case.* The interface of the homodimer complex 1E2D (left) features a

292 compact and planar core composed of a single patch of atoms with high shelling

293 orders (large panel), which the MD simulations of Mihalek and coworkers also

294 identify as dry (lower left-hand panel). Such compact interfaces with disk-like

295 topologies and no holes represent best case scenarios for the predictive power

296 of our model. Also conservation performs well for this complex. However, in

297 contrast to shelling order, the conservation score delimitates a patch which

298 extends far beyond the dry residues, resulting in a good sensitivity but a

299 poor selectivity. In fact, the most highly conserved residues are catalytic in

300 nature, and located at the entrance of a finger-like cavity which extends, from

301 the other side of the protein, in the direction of the interface (not visible

302 in the figure). The co-crystallized thymidine monophosphate and adenosine

303 diphosphate substrates [38] allowed Mihalek and coworkers to identify these

304 residues as catalytic and as such to exclude them from their analysis. However,

305 the detection of catalytic residues is not always as straightforward and the

306 influence of this and a variety of other factors hamper the use of conservation

307 measures for specific predictions.

308 *Stacks of water molecules.* The interface of the homodimer 1L5W is quite

309 extensive and highly non planar, consisting of two 'prongs' separated by a cleft.

310 Two high-VSO patches are found on either of the prongs. The *ABW* interface

15

³¹¹ is discontinuous in the region of the cleft, due to the presence of more than

³¹² one layer of solvent molecules sandwiched between the partners (Figure 9);

³¹³ this resets the shelling order to low values in that area. On the other hand,

³¹⁴ MD simulations find a much smaller patch of dry residues that extends inside

³¹⁵ the cleft, which means that some of the aforementioned solvent molecules

³¹⁶ are in fact structural in nature, and do not move during the simulation. A

³¹⁷ remarkable example of this occurs for tryptophane 203 (located inside the

³¹⁸ cleft), which is classified as dry by Mihalek and coworkers but is surrounded by

³¹⁹ numerous water molecules on Figure 9. Here we are confronted with the main

³²⁰ advantage of MD simulations over our model: they are able to discriminate

³²¹ structural water on the basis of residence times, whereas our static model

³²² relies on the fact that buried interfacial water does not usually form multiple

³²³ layers. However, it is clear from Tables 1 and 2 that situations featuring water

³²⁴ molecules structured along more than one layer rarely occur; we discuss this

³²⁵ issue further in section 4. Within the interface, conservation fares better since

³²⁶ one of the prongs and the cleft region are fairly well conserved. However, the

³²⁷ most conserved regions lie at the protein core (not visible on the figure) and,

³²⁸ to a lesser extent, elsewhere on the protein surface.

³²⁹ *Discontinuities of the interface.* Figure 8 shows a graphical representation

³³⁰ of shelling, conservation and dryness for complex 1A59. 1A59 has an intri-

³³¹ cate topology, consisting of two monomers of predominantly globular nature

³³² linked by long 'tails' wrapped around the partner. Dry residues appear both

³³³ on the globular part and on the first segment of the tail (Figure 8). Voronoi

³³⁴ shelling order very accurately predicts the latter patch of dry residues, but

³³⁵ over-predicts the entire tail as being dry or active, too. More interestingly, it

³³⁶ also misses the lower part of the dry patch on the globular side of the protein.

16

337 A careful inspection of the interface reveals two holes in the AB interface which

338 reset the shelling order there, preventing the shelling order from peaking in

339 this region (Figure 10). The fact that such holes are visible in the AB interface

340 hints at a sizable packing issue: minute defects do not usually result in such

341 discontinuities of the AB interface[27]. Indeed, the gaps between the atoms of

342 the two monomers [1] span the range 5.2-6.2 Å and 5.9-6.3 Å, respectively, and

343 could accommodate a water molecule each. Since the crystal structure does

344 not contain structural water, we cannot ascertain whether this is the case and

345 our fast solvation procedure proved unable to fill the holes – even though it

346 did successfully place isolated water molecules in three other locations. By

347 comparison, conservation correlates with dryness on the globular part of the

348 interface, but also features widespread conserved patches covering most of the

349 protein surface.

---

[1] Hole 1: residues 209 to 213 (chain A) and 583 to 587 (chain B); hole 2: residues 206 to 210 (chain A) and 586 to 590 (chain B).

4 DISCUSSION AND CONCLUSION

4.1 A quantitative interface definition

Among the various definitions of what exactly constitutes a protein-protein interface, the planar facets obtained from a Voronoi tessellation [39,40] arguably present the closest ties to the literal meaning of the term 'interface'. Indeed, such facets stem from pairs of directly interacting atoms, and the definition of the interaction area is simpler than that required by analytical interface models [41]. The Voronoi model shows excellent correlation with classically defined curvature and solvent accessible area but captures the interface more fully than methods based on solvent accessibility [27] —see also [42] for a review on the use of Voronoi diagrams in protein structure and interface analysis. By contrast, the widely used geometric footprint (based on residue contacts) yields an ambiguous interaction layer biased towards large residues and subject to an arbitrary distance cut-off [3].

Here, we go beyond the binary classification of whether or not a given atom is part of the interface and furthermore quantify how many facets separate it from the edge of the interface. The idea is related to the concept of residue or atom depth [43,44] which shows some correlation with thermodynamic properties [43] and residue conservation [45] in globular proteins. Previous studies have defined atomic depth as the simple Euclidean distance to the closest solvent molecule. By contrast, Voronoi shelling order partitions the interface into concentric shells, accounting for both the geometry and topology of the interface and appears closer to physical reality. Yet other previous studies have dissected protein interfaces into "inner" and "outer" or "core" and "rim" residues

18

374 (for example, [46–48,36]). Although a number of general trends emerge, con-

375 clusions from these works are hindered by distinct definitions of the interface

376 combined with different classifications for core and rim. Voronoi shelling order

377 provides a more quantitative, parameter-free and unambiguous alternative to

378 the ad-hoc classifications previously employed.

379 *4.2 Shelling order and water dynamics*

380 The shelling of the Voronoi interface yields an accurate quantification for the

381 concept of burial depth. Shelling order quantifies the number of atomic shells

382 a water molecule must pass on the shortest path to a given position (facet) in

383 the interface. This description is particularly valuable for highly curved inter-

384 faces (1A59, 1L5W...) which the Euclidean distance cannot correctly measure.

385 We have here revealed a clear correlation between Voronoi shelling order and

386 the 'dryness' of a residue, that is, its shielding from itinerant bulk solvent

387 molecules. While one could expect some ties between the two measures, the

388 extent of the agreement over a representative set of complexes is intriguing.

389 After all, dryness was derived from exhaustive molecular dynamics simulations

390 which consider hundreds of additional parameters and details that are totally

391 ignored by our model. On the contrary, Voronoi shelling order is a purely

392 geometric property, calculated from a static set of atomic positions without

393 any further parameter. In particular, we do *not* consider: electrostatic charges,

394 polarity, hydrogen bonds, or any kind of fluctuations – all of which are ex-

395 pected to influence water dynamics. This suggests that the seemingly complex

396 dynamic exchange of bulk solvent with interfacial water primarily depends on

397 a simple path length and could tentatively be approximated by an analytical

19

398 model of diffusion along a gradient.

4.3 Complementarity of conservation and Voronoi shelling order

400 Evolutionary conservation alone cannot usually be employed to predict the
401 active part of an interface, let alone the interface itself. Hence the neces-
402 sity to cross-correlate it with some other measure (like geometric footprint or
403 change in solvent accessibility) before using it for such purposes. By compar-
404 ison, Voronoi shelling order simultaneously offers an unambiguous definition
405 of the protein-protein interface and a more fine-grained classification within
406 this interface.

407 Furthermore, the quantification of evolutionary signals is not trivial. pFam
408 sequence alignments are considered high quality but are not guaranteed to be
409 homogeneously distributed between protein families, hereby introducing bias.
410 Moreover, some protein stretches cannot be aligned at all, and needed to be
411 excluded from our analysis of conservation. We quantify conservation with an
412 entropy-based measure that has been shown to outperform other conservation
413 scores [35]; alternative means can be employed but the actual method of choice
414 seems to have limited effect on the correlation with dryness[26].

415 Bearing in mind the interference from many other factors, sequence conserva-
416 tion can, nevertheless, provide independent testimony of an area's importance.
417 It confirms the notion of water shielding as an indicator of binding activity
418 and it supports the functional relevance of shelling order. In fact, conservation
419 and VSO are best used in conjunction rather than as competitors. We find a
420 general correlation between shelling order and conservation but, in contrast to

20

421 a simple classification into rim and core, our continuous measure also resolves

422 interesting deviations from this trend. Such deviations hint at catalytic sites,

423 defects in solvation and packing, but may also indicate binding contributions

424 that do not directly rely on water shielding.

425 *4.4   Methodological improvements*

426 As previously discussed, discrepancies between dryness and shelling order arise

427 for cases where structural (slow moving) water molecules form more than

428 one layer inside a cavity. This is due to the fact that in our current model,

429 interfacial water molecules must make simultaneous contact with both protein

430 partners; any additional layer of water molecules not fulfilling this criterion

431 will be considered as bulk and lead to the splitting of the ABW interface.

432 However, 'trapped' water molecules are known to stabilize turns and bends

433 through hydrogen bonding with main-chain atoms in otherwise unstructured

434 regions [49], and cannot be ignored. Their behavior is so different from that of

435 bulk water that it is debatable whether they should be considered as delimiters

436 for the interface, even when stacked in more than one layer – dryness results

437 from MD simulations tend to show that they shouldn't.

438 The most straightforward approach to alleviate discrepancies between dryness

439 and shelling order in these difficult cases would be to optimize the threshold

440 separating 'dry' from 'wet', instead of using Mihalek's choice [26]. Our model

441 could also be extended so as to declare as interface water all solvent molecules

442 W_i found on a path $AW_1 \ldots W_k B$ joining both partners. Using $k = 2$ or $k = 3$

443 could allow to infer similar properties for water molecules organized in layers,

444 as in complex 1L5W. Nevertheless, the current interface model, despite using

21

445 $k = 1$, demonstrates that it is legitimate to infer dryness/activity from a

446 purely geometric perspective. This effectively replaces a costly MD simulation

447 by a very fast computation on a structure taken directly from the PDB.

448 Another worthwhile methodological improvement would address rare cases

449 where discontinuities in the interface appear due to packing or solvation de-

450 fects. An example thereof is the previously discussed 1A59 interface (Fig-

451 ure 10). Regardless of the quality of the structure or the equilibration proce-

452 dure, such cases could be accommodated by using a water probe radius larger

453 than 1.4 Å, or by devising an adaptive scheme for the value of α ($\alpha > 0$)

454 employed to construct the α-complex. In any case, these extensions should be

455 investigated in conjunction with the threshold used to define dryness.

456 ## 4.5   Conclusion

457 In this paper, we present a novel method to explore protein-protein interfaces.

458 The interface is defined using the Voronoi diagram of interacting atom pairs;

459 unlike geometric footprinting methods, all atoms involved in the interface are

460 identified with little to no over-prediction and without resorting to a distance

461 threshold. We have shelled the Voronoi interface from the rim to the core, thus

462 associating an interface depth to each atom. This Voronoi shelling order (VSO)

463 correlates very well with the protection of residues from itinerant water fluxes,

464 as computed by Mihalek and coworkers [26] which, in turn, can be considered

465 a measure of residue activity. The calculation of shelling orders, however, is

466 about five orders of magnitude faster than a typical MD simulation. Moreover,

467 the rather accurate prediction from a simplistic and purely geometric model

468 hints at the possibility to approximate the complex dynamics of interfacial

22

469 water by simple analytic diffusion models. Comparison with evolutionary sig-

470 nals confirms the functional relevance of 'dry' residues and, likewise, reveals

471 a general increase of conservation towards inner interface shells. Systematic

472 deviations from this trend may inform about distinct binding mechanisms,

473 catalytic activities but also modeling errors. Our accurate and continuous

474 scale of burial depths could also be used to delimitate patches on an interface.

475 Hence, it appears as a worthy candidate for the theoretical study of collective

476 effects in protein-protein interfaces [13], which are progressively replacing the

477 traditional 'hotspot' view.

5 METHODS

5.1 Complex preparation

The coordinates for the homo- and heterodimer complexes listed in Tables 1 and 2 originate from the PDB database. Crystallographic water molecules were removed in order to exclude bias from different structure qualities. Missing atoms, including polar hydrogens, were added and briefly minimized. The structure was surrounded by a 9 Å layer of water molecules from an equilibrated TIP3P box. The water was briefly minimized by 3 rounds of conjugate-gradient optimization of 40 steps each with, initially (round 1), frozen and later (rounds 2 and 3) harmonically restrained protein coordinates. Keeping this restraint, the water was then further relaxed by 100 2-fs steps of molecular dynamics at 100 K, followed by 40 steps conjugate gradient minimization. Optimizations and simulations were performed using the CHARMM19 force field [50] and an electrostatic cutoff of 12 Å with force shifting [51] inside the X-PLOR package. This structure preparation protocol is automated by the pdb2xplor.py program which is part of the open source Biskit package [52]. The final structure was stripped of its hydrogen atoms and used as input for the Voronoi interface calculations (see below).

To test the legitimacy of this economical solvation procedure, a more thorough approach was employed on complex 1M0S. After an initial re-optimization of the crystal structure (retaining crystal water), the complex was placed inside a triclinic box, solvated with SPC water molecules from an equilibrated box and neutralized by 8 Na^+ ions. The solvent molecules were then relaxed around the fixed solute by a steepest-descent optimization followed by 100 ps

24

of molecular dynamics (MD) simulation with position restraints on the solute. The entire system was then simulated for 5 ns without restraints, with a 300 K Maxwellian distribution of initial velocities. MD simulations employed the particle-mesh Ewald treatment of long-range electrostatics and periodic boundary conditions, as well as couplings to heat (300 K, 1 ps) and pressure (1 bar, 1 ps) baths; they were performed with GROMACS 3.3.2 [53] using the OPLS all-atom force field [54]. The final equilibrated box had dimensions 76x92x69 Å and comprised 13460 water molecules. Convergence of the protein structure was reached after 2 ns of simulation, at a mean RMSD of 1.90 Å from the crystal structure.

Section A.2 of Supplemental Material compares the Voronoi interfaces of complex 1M0S using these two equilibration procedures. The very similar results, both in terms of interface topology and the identification of interfacial water, justify the economical solvation method and indicate the robustness of our model against minor changes both in protein conformation and hydration patterns.

5.2   Calculation of shelling orders

The program Intervor, responsible for the actual computation and shelling of the Voronoi interface, is based on the CGAL computational geometry library [55]; an online version of Intervor is available [56]. On an Intel Pentium IV 3 GHz CPU, an Intervor run for a typical complex takes less than 5 seconds. We also provide a wrapper (Biskit.Intervor) for integrating the stand-alone program in Biskit workflows. Residue shelling orders were calculated by averaging over a residue's interface atoms.

25

5.3 Dryness and conservation

Dryness results were those discussed in [26] and were kindly provided to us by O. Lichtarge and coworkers.

Multiple sequence alignments were obtained from the pFam database [33] of HMMER profiles [34] using the HMMER software version 2.3.1. Protein family profiles matching a given sequence were identified with hmmpfam using a conservative E-value and bit score cutoff of 1e-8 and 60, respectively. The sequence was then aligned to the matching profile with the hmmalign program. Following [35], the conservation of each alignment position was quantified by the Kullback-Leibler divergence (relative entropy) between the HMM emission probabilities p and the background distribution of amino acids in SwissProt q:

$$s = \sum_{i=1}^{20} p_i \log \frac{p_i}{q_i}.$$

The complete procedure is automated in the Hmmer.py module of Biskit. Before further analysis, residues outside the interface (average $VSO = 0$) or lacking conservation scores were removed and conservation scores were independently normalized to the maximum of each monomer face.

5.4 ROC curves

Receiver Operating Characteristics (ROC) curves[57] are an efficient way of representing the accuracy of a binary classifier. A binary classifier maps instances of an object into two categories, positive or negative, based on each instance's position relative to a threshold. The quality of the classifier is then assessed by how well the prediction relates to the actual value of the instance.

26

Four cases are possible: true positive (both the outcome from a prediction and the actual value are positive), false positive (the prediction is positive while the actual value is negative), true negative (prediction and value are both negative) and false negative (prediction is negative while value is positive). From this contingency table, the notions of selectivity and sensitivity can be defined as

$$Sensitivity = \frac{True\ Positive}{True\ Positive + False\ Negative}$$

and

$$Specificity = \frac{True\ Negative}{True\ Negative + False\ Positive}.$$

A ROC curve is the 2D plot of sensitivity versus specificity, where each point corresponds to a different threshold value. A perfect predictor, which features neither false positive nor false negative occurrences, should pass through the point (1,1) for the optimal threshold value. Therefore, the closer the ROC plot is to the upper right corner, the higher the overall accuracy of the test [58]. A purely random classifier, with equal chances of making correct or erroneous predictions, has a linear ROC curve connecting points (0,1) and (1,0) – the first diagonal. How much better than random a predictor is can hence be quantified by calculating the area between its ROC curve and the diagonal, which varies from -0.5 (worst-case classifier) to 0.5 (perfect classifier) through 0 (pure random classifier). ROC curve and ROC area calculations were performed with the Biskit.ROCalyzer module.

By way of example, figure 4 shows typical ROC curves for shelling order and conservation as predictors for dryness, in the specific case of the 1HE1 complex. For this system, shelling order is systematically better than conservation at

27

predicting dryness, regardless of the threshold chosen to discriminate between positive and negative predictions in each case. This translates into a larger area between the diagonal (representing a random prediction) and the shelling order ROC plot, than between the diagonal and the conservation ROC plot.

5.5 Miscellaneous

The Biskit python package [52] was also used for various other scripting tasks and the collation of results. All parts of Biskit are open source and available at http://biskit.sf.net. Pymol [59], Ipe [60] and CGAL-Ipelets [61] were employed for the rendering of figures.

References

[1] A.-C. Gavin, P. Aloy, P. Grandi, R. Krause, M. Boesche, M. Marzioch, C. Rau, L. J. Jensen, S. Bastuck, B. Dmpelfeld, A. Edelmann, M.-A. Heurtier, V. Hoffman, C. Hoefert, K. Klein, M. Hudak, A.-M. Michon, M. Schelder, M. Schirle, M. Remor, T. Rudi, S. Hooper, A. Bauer, T. Bouwmeester, G. Casari, G. Drewes, G. Neubauer, J. M. Rick, B. Kuster, P. Bork, R. B. Russell, G. Superti-Furga, Proteome survey reveals modularity of the yeast cell machinery., Nature 440 (7084) (2006) 631–636.

28

582   URL `http://dx.doi.org/10.1038/nature04532`

583 [2] J. J. Gray, High-resolution protein-protein docking., Curr Opin Struct Biol
584   16 (2) (2006) 183–193.
585   URL `http://dx.doi.org/10.1016/j.sbi.2006.03.003`

586 [3] R. Grünberg, J. Leckner, M. Nilges, Complementarity of structure ensembles
587   in protein-protein binding., Structure 12 (12) (2004) 2125–2136.
588   URL `http://dx.doi.org/10.1016/j.str.2004.09.014`

589 [4] R. Grünberg, M. Nilges, J. Leckner, Flexibility and conformational entropy in
590   protein-protein binding., Structure 14 (4) (2006) 683–693.
591   URL `http://dx.doi.org/10.1016/j.str.2006.01.014`

592 [5] C. Chotia, J. Janin, Principles of protein-protein recognition, Nature 256 (1975)
593   705–708.

594 [6] J.-L. K. Kouadio, J. R. Horn, G. Pal, A. A. Kossiakoff, Shotgun alanine scanning
595   shows that growth hormone can bind productively to its receptor through a
596   drastically minimized interface., J Biol Chem 280 (27) (2005) 25524–25532.
597   URL `http://dx.doi.org/10.1074/jbc.M502167200`

598 [7] S. Jones, J. Thornton, Analysis of protein-protein interaction sites using surface
599   patches, J. Mol. Biol. 272.

600 [8] B. Ma, T. Elkayam, H. Wolfson, R. Nussinov, Protein-protein interactions:
601   Structurally conserved residues distinguish between binding sites and exposed
602   protein surfaces, Proceedings of the National Academy of Sciences 100 (10)
603   (2003) 5772–5777.
604   URL `http://www.pnas.org/cgi/content/abstract/100/10/5772`

605 [9] L. Lo Conte, C. Chothia, J. Janin, The atomic structure of protein-protein
606   recognition sites, Journal of Molecular Biology 285 (1999) 2177–2198.

607   URL   `http://www.sciencedirect.com/science/article/`

608   `B6WK7-45R884M-RY/2/6f4a9866e2495a34273695de046893dc`

[10] S. A. Teichmann, Principles of protein-protein interactions, Bioinformatics 18 (suppl. 2) (2002) S249–.

     URL   `http://bioinformatics.oxfordjournals.org/cgi/content/` `abstract/18/suppl_2/S249`

[11] T. Clackson, J. Wells, A hot spot of binding energy in a hormone-receptor interface, Science 267 (5196) (1995) 383–386.

     URL `http://www.sciencemag.org/cgi/content/abstract/267/5196/383`

[12] I. S. Moreira, P. A. Fernandes, M. J. Ramos, Hot spots – a review of the protein-protein interface determinant amino-acid residues, Proteins: Structure, Function, and Bioinformatics 68 (4).

     URL `http://dx.doi.org/10.1002/prot.21396`

[13] D. Reichmann, O. Rahat, S. Albeck, R. Meged, O. Dym, G. Schreiber, The modular architecture of protein-protein binding interfaces, PNAS 102 (1) (2005) 57–62.

     URL `http://www.pnas.org/cgi/content/abstract/102/1/57`

[14] D. Reichmann, O. Rahat, M. Cohen, H. Neuvirth, G. Schreiber, The molecular architecture of protein-protein binding sites, Current Opinion in Structural Biology 17 (2007) 67–76.

[15] D. R. Caffrey, S. Somaroo, J. D. Hughes, J. Mintseris, E. S. Huang, Are protein-protein interfaces more conserved in sequence than the rest of the protein surface?, Protein Sci 13 (1) (2004) 190–202.

     URL `http://www.proteinscience.org/cgi/content/abstract/13/1/190`

[16] B. E. Shakhnovich, N. V. Dokholyan, C. DeLisi, E. I. Shakhnovich, Functional fingerprints of folds: Evidence for correlated structure-function evolution,

30

Journal of Molecular Biology 326 (1) (2003) 1–9.

URL http://www.sciencedirect.com/science/article/
B6WK7-47RC32Y-3/2/780a30e8b2d84bdefba0ea80b0a6b6b2

[17] A. Valencia, Automatic annotation of protein function, Current Opinion in
Structural Biology 15 (3) (2005) 267–274.

URL http://www.sciencedirect.com/science/article/
B6VS6-4G7X9HS-3/2/90d887674957c53860854c3254a94748

[18] P. Aloy, H. Ceulemans, A. Stark, R. B. Russell, The relationship between
sequence and interaction divergence in proteins, Journal of Molecular Biology
332 (5) (2003) 989–998.

URL http://www.sciencedirect.com/science/article/
B6WK7-49HMCGT-4/2/6d13750d3d40cc10b07ef096ef54961b

[19] R. P. Bahadur, P. Chakrabarti, F. Rodier, J. Janin, A dissection of specific and
non-specific protein-protein interfaces, Journal of Molecular Biology 336 (4)
(2004) 943–955.

URL http://www.sciencedirect.com/science/article/
B6WK7-4BRTKR9-C/2/ce716dee1132d2605f8e1c96d1154253

[20] O. Lichtarge, H. R. Bourne, F. E. Cohen, An evolutionary trace method defines
binding surfaces common to protein families, Journal of Molecular Biology
257 (2) (1996) 342–358.

URL http://www.sciencedirect.com/science/article/
B6WK7-45PV59P-1T/2/08c0824641e25a3fe8dba3e81635a653

[21] O. Rahat, A. Yitzhaky, G. Schreiber, Cluster conservation as a novel tool for
studying protein-protein interactions evolution., Proteins.

URL http://dx.doi.org/10.1002/prot.21749

[22] F. Rodier, R. Bahadur, P. Chakrabarti, J. Janin, Hydration of protein - protein

31

659   interfaces, Proteins 60 (1) (2005) 36–45.

660   [23] A. A. Bogan, K. S. Thorn, Anatomy of hot spots in protein interfaces, Journal

661   of Molecular Biology 280 (1998) 1–9.

662   URL   http://www.sciencedirect.com/science/article/

663   B6WK7-45S49GB-9C/2/b3d9c6f299c1eec3933d2774dffaf67d

664   [24] A. Fernandez, R. S. Berry, Extent of Hydrogen-Bond Protection in Folded

665   Proteins: A Constraint on Packing Architectures, Biophys. J. 83 (5) (2002)

666   2475–2481.

667   URL http://www.biophysj.org/cgi/content/abstract/83/5/2475

668   [25] A. Fernandez, H. A. Scheraga, Insufficiently dehydrated hydrogen bonds as

669   determinants of protein interactions, Proceedings of the National Academy of

670   Sciences 100 (1) (2003) 113–118.

671   URL http://www.pnas.org/cgi/content/abstract/100/1/113

672   [26] I. Mihalek, I. Res, O. Lichtarge, On itinerant water molecules and detectability

673   of protein-protein interfaces through comparative analysis of homologues,

674   Journal of Molecular Biology 369 (2) (2007) 584–595.

675   [27] F. Cazals, F. Proust, R. P. Bahadur, J. Janin, Revisiting the Voronoi description

676   of protein-protein interfaces, Protein Sci 15 (9) (2006) 2082–2092.

677   URL http://www.proteinscience.org/cgi/content/abstract/15/9/2082

678   [28] F. M. Richards, The interpretation of protein structures: Total volume, group

679   volume distributions and packing density, Journal of Molecular Biology 82

680   (1974) 1–14.

681   [29] F. Aurenhammer, Power diagrams: properties, algorithms and applications,

682   SIAM J. Comput. 16 (1987) 78–96.

683   [30] C. Chotia, The nature of accessible and buried surfaces in proteins, J. Mol. Bio.

684   105 (1976) 1–12.

[31] B. Lee, F. M. Richards, The interpretation of protein structures: Estimation of static accessibility, Journal of Molecular Biology 55 (3) (1971) 379–380.

URL `http://www.sciencedirect.com/science/article/B6WK7-4DNGV9F-34/2/659a5209b127663bc3133c0b801a29a5`

[32] H. Edelsbrunner, E. P. Mücke, Three-dimensional alpha shapes, ACM Trans. Graph. 13 (1) (1994) 43–72.

[33] R. D. Finn, J. Mistry, B. Schuster-Bockler, S. Griffiths-Jones, V. Hollich, T. Lassmann, S. Moxon, M. Marshall, A. Khanna, R. Durbin, S. R. Eddy, E. L. L. Sonnhammer, A. Bateman, Pfam: clans, web tools and services, Nucl. Acids Res. 34 (suppl. 1) (2006) D247–251.

URL `http://nar.oxfordjournals.org/cgi/content/abstract/34/suppl_1/D247`

[34] R. Durbin, S. Eddy, A. Krogh, G. Mitchison, Biological sequence analysis: probabilistic models of proteins and nucleic acids, Cambridge University Press, 1998, Ch. The theory behind profile HMMs.

[35] K. Wang, R. Samudrala, Incorporating background frequency improves entropy-based residue conservation measures., BMC Bioinformatics 7 (2006) 385.

URL `http://dx.doi.org/10.1186/1471-2105-7-385`

[36] M. Guharoy, P. Chakrabarti, Conservation and relative importance of residues across protein-protein interfaces., Proc Natl Acad Sci U S A 102 (43) (2005) 15447–15452.

URL `http://dx.doi.org/10.1073/pnas.0505425102`

[37] T. Selzer, G. Schreiber, Predicting the rate enhancement of protein complex formation from the electrostatic energy of interaction., J Mol Biol 287 (2) (1999) 409–419.

URL `http://dx.doi.org/10.1006/jmbi.1999.2615`

[38] N. Ostermann, I. Schlichting, R. Brundiers, M. Konrad, J. Reinstein, T. Veit, R. S. Goody, A. Lavie, Insights into the phosphoryltransfer mechanism of human thymidylate kinase gained from crystal structures of enzyme complexes along the reaction coordinate, Structure 8 (6) 629–642.
   URL http://www.sciencedirect.com/science/article/ B6VSR-40H578S-B/2/72acba30cd1e54cc5111cf865a8374b2

[39] A. Varshney, F. P. Brooks, D. C. Richardson, W. V. Wright, D. Manocha, Defining, computing, and visualizing molecular interfaces, in: IEEE Visualization, Atlanta, USA, 1995, pp. 36–43.

[40] Y.-E. A. Ban, , H. Edelsbrunner, J. Rudolph, Interface surfaces for protein-protein complexes, in: RECOMB, San Diego, 2004, pp. 205–212.

[41] R. R. Gabdoulline, R. C. Wade, D. Walther, Molsurfer: A macromolecular interface navigator., Nucleic Acids Res 31 (13) (2003) 3349–3351.

[42] A. Poupon, Voronoi and voronoi-related tessellations in studies of protein structure and interaction., Curr Opin Struct Biol 14 (2) (2004) 233–241.
   URL http://dx.doi.org/10.1016/j.sbi.2004.03.010

[43] S. Chakravarty, R. Varadarajan, Residue depth: a novel parameter for the analysis of protein structure and stability., Structure 7 (7) (1999) 723–732.

[44] A. Pintar, O. Carugo, S. Pongor, Atom depth in protein structure and function., Trends Biochem Sci 28 (11) (2003) 593–597.

[45] A. Pintar, O. Carugo, S. Pongor, Atom depth as a descriptor of the protein interior., Biophys J 84 (4) (2003) 2553–2561.

[46] P. Chakrabarti, J. Janin, Dissecting protein-protein recognition sites, Proteins 47.

[47] I. M. A. Nooren, J. M. Thornton, Structural characterisation and functional

significance of transient protein-protein interactions., J Mol Biol 325 (5) (2003) 991–1018.

[48] A. Bordner, R. Abagyan, Statistical analysis and prediction of protein-protein interfaces, Proteins 60 (3) (2005) 353–66.

[49] J. G. S. Sheldon Park, Statistical and molecular dynamics studies of buried waters in globular proteins, Proteins: Structure, Function, and Bioinformatics 60 (2005) 450–463.
URL http://dx.doi.org/10.1002/prot.20511

[50] B. Brooks, R. Bruccoleri, Olafson B.D., D. States, S. Swaminathan, M. Karplus, CHARMM: a program for macromolecular energy, minimization and dynamics calculations., J Comp Chem 4 (1983) 187–217.

[51] P. Steinbach, R. Loncharich, B. Brooks, The effects of environment and hydration on protein dynamics: A simulation study of myoglobin., Chem Phys 158 (1991) 383–94.

[52] R. Grünberg, M. Nilges, J. Leckner, Biskit–A software platform for structural bioinformatics, Bioinformatics 23 (6) (2007) 769–770.
URL http://bioinformatics.oxfordjournals.org/cgi/content/abstract/23/6/769

[53] D. V. D. Spoel, E. Lindahl, B. Hess, G. Groenhof, A. E. Mark, H. J. C. Berendsen, Gromacs: fast, flexible, and free., J Comput Chem 26 (16) (2005) 1701–1718.
URL http://dx.doi.org/10.1002/jcc.20291

[54] W. Damm, A. Frontera, J. Tirado-Rives, W. L. Jorgensen, Opls all-atom force field for carbohydrates, Journal of Computational Chemistry 18 (1997) 1955–1970.

35

761   URL http://dx.doi.org/10.1002/(SICI)1096-987X(199712)18:16⟨1955::

762   AID-JCC1⟩3.0.CO;2-L

763 [55] Cgal, Computational Geometry Algorithms Library, http://www.cgal.org.

764 [56] http://cgal.inria.fr/Intervor.

765 [57] D. M. Green, J. M. Swets, Signal detection theory and psychophysics, John

766   Wiley and Sons Inc., New York, 1966.

767 [58] M. Zweig, G. Campbell, Receiver-operating characteristic (ROC) plots: a

768   fundamental evaluation tool in clinical medicine [published erratum appears

769   in Clin Chem 1993 Aug;39(8):1589], Clin Chem 39 (4) (1993) 561–577.

770   URL http://www.clinchem.org/cgi/content/abstract/39/4/561

771 [59] W. DeLano, The Pymol molecular graphics system, http://www.pymol.org

772   (2002).

773 [60] O. Cheong, The Ipe extensible drawing editor, http://tclab.kaist.ac.kr/

774   ipe/ (1993-2007).

775 [61] http://cgal-ipelets.gforge.inria.fr/.

36

6   FIGURES LEGENDS

Legend of Fig. 1. Voronoi diagram (light solid lines) for a hypothetical molecule consisting of four atoms (a_1 to a_4), and restriction of the balls to their Voronoi regions. The α-complex ($\alpha = 0$) consists of the four vertices a_1 to a_4, of the three edges a_1a_2, a_1a_3, a_2a_3, and of the triangle $a_1a_2a_3$ formed between them.

Legend of Fig. 2. (a) Shelling of the Voronoi interface of a dimer complex, seen from the top. Solid dots represent protein atoms' centers, hollow dots water atoms' centers; for clarity, all atomic radii have been taken equal and the corresponding spheres omitted. The Voronoi facets composing the protein-protein interface are colored according to their shelling order: one (light gray, at the rim), two (middle gray), three (dark gray). (b) Two-dimensional illustration of the Voronoi interface shelling of a dimer complex. Red and blue circles represent the atoms of each partner, the green circle a water molecule. Interface Delaunay edges, which connect atoms on different partners, are shown as solid black (AB interface) or green ($AW - BW$ interface) lines; the Voronoi facets are shown as dashes. Black numerals denote the shelling order of each Delaunay edge/Voronoi facet, from which the atomic shelling orders (red, blue and green numerals) can be derived (refer to text for details). On this simple illustration, the high curvature of the $AW - BW$ interface due to the water molecule accounts for the high shelling order of the blue atoms.

Legend of Fig. 3. (a) Voronoi interface of the 2DOR homodimer complex, superimposed on the solvent accessible surface representation of one of the monomers (gray); for clarity, the second monomer is not shown. The facet

37

shelling order varies from 1 (blue) to 6 (red). (b) Solvent accessible surface of one monomer of the 2DOR complex, showing the shelling order of interface atoms (color-coded as in panel b).

Legend of Fig. 4. ROC plots evaluating shelling order (solid line) and conservation (dashed line) as predictors for dryness. Each point on a ROC plot corresponds to a different threshold value for the prediction. The plot for a perfect predictor should pass through $(1, 1)$; that of a random predictor (on average) is the diagonal (dotted line). The area between the ROC curve and the diagonal measure the performance of the predictor compared to random.

Legend of Fig. 5. Performance of shelling order (circles, solid line) and conservation (squares, dashed line) as predictors of dryness, for all studied heterodimer (left panel) and homodimer (right panel) complexes. Scores are measured as the area between the corresponding ROC curve and the diagonal; complexes are sorted by decreasing shelling order score. Negative values (hatched area) denote a performance that is no better (on average) than that of a purely random classifier.

Legend of Fig. 6. Spatial distribution of conservation across heterodimer interfaces. The conservation score for each interface residue, normalized to the maximum score, is plotted against its normalized shelling order. Black –: running average with a large window size (1/4 of all interface residues); Gray –: all data points; $- \cdot -$: Integral over running average; $\cdots$: Double integral over running average; Δ: deviation of the double integral from 0.5 – values below zero indicate conservation bias towards high shelling order (the core).

Legend of Fig. 7. Spatial distribution of conservation across homodimer interfaces. See figure 6 and text for a detailed description.

38

Legend of Fig. 8. Projection of shelling order (large panels), dryness (lower left-hand panel) and conservation (lower right-hand panel) on the molecular surface of homocomplexes 1E2D (left), 1L5W (center) and 1A59 (right); one of the monomers was removed for clarity. Cold (resp. hot) colors represent low (resp. high) values; gray areas denote residues for which conservation information was unavailable.

Legend of Fig. 9. View of the cleft region of the 1L5W interface, showing the two protein partners as solid and mesh surfaces, respectively. Colors code for shelling order, which is low inside the cleft due to the presence of numerous water molecules which fragment the interface.

Legend of Fig. 10. Boundary of the AB interface of complex 1A59 (red line), interfacial water (gray spheres), and $AW - BW$ interface (grey and green Voronoi polygons). The holes pointed out by arrows prevent the shelling order from peaking in the middle of the interface patch –compare to the bottom left panel of complex 1A59 on Fig. 8.

7 TABLES

PDB Id.	VSO → dry	Conservation → dry	Conservation → VSO
1HE1	0.42	0.28	0.02
1CXZ	0.39	0.24	0.19
1CEE	0.39	0.12	0.11
1C1Y	0.36	0.17	0.05
1RRP	0.34	0.22	0.21
1FIN	0.34	0.10	0.18
1E96	0.34	-0.02	0.15
1ZBD	0.33	0.09	0.19
1FOE	0.33	0.19	0.27
1A0O	0.32	0.23	0.12
2TRC	0.32	-0.08	0.11
1GOT	0.32	0.13	0.23
1WQ1	0.31	0.19	0.08
1IBR	0.30	0.01	-0.14
1A2K	0.26	0.15	0.28
1LFD	0.25	0.26	0.15
1AGR	0.19	0.10	0.25
1YCS	0.16	0.16	0.29
avg.	0.31	0.14	0.15

Table 1

Heterodimers. Performance of shelling order (VSO) as a predictor for dryness, of conservation as a predictor for dryness, and of conservation as a predictor for shelling order, for each of the considered heterodimer complexes.

40

PDB Id.	VSO → dry	Conservation → dry	Conservation → VSO
2BIF	0.45	0.09	0.02
1E5Q	0.45	0.15	0.31
1E2D	0.45	0.37	0.38
1H7T	0.45	0.12	0.17
1TB5	0.43	0.14	0.02
2DOR	0.42	0.19	0.13
1QIN	0.42	0.14	0.14
1E98	0.42	0.40	0.45
1J79	0.40	-0.09	-0.08
1NYW	0.40	-0.09	0.04
1BTO	0.38	0.27	0.12
1Y6R	0.38	0.17	0.03
1KER	0.37	0.14	0.08
1EK4	0.37	0.15	0.21
1LBX	0.37	0.21	0.11
1L9W	0.36	0.29	0.27
1AI2	0.36	0.18	-0.05
1W1U	0.35	0.07	-0.03
1DQX	0.33	0.10	-0.09
1E7Y	0.32	0.24	-0.06
1HKV	0.32	0.09	0.04
1M0S	0.32	0.07	0.34
1KC3	0.32	0.35	0.32
1M4N	0.31	0.17	0.14
1A59	0.31	0.15	0.19
1DQR	0.31	0.09	0.08
1AN9	0.30	0.11	0.06
1M7P	0.29	0.01	0.08
1TC2	0.29	-0.01	0.17
1AD3	0.28	-0.03	0.16
1ALN	0.27	0.14	0.04
1H16	0.27	-0.06	-0.02
1M9N	0.26	0.09	0.20
1L5W	0.24	0.18	0.25
1CG0	0.22	0.12	0.05
1LXY	0.21	0.10	0.11
avg.	0.34	0.13	0.12

Table 2

Homodimers. Performance of shelling order (VSO) as a predictor for dryness, of conservation as a predictor for dryness, and of conservation as a predictor for shelling order, for each of the considered homodimer complexes.
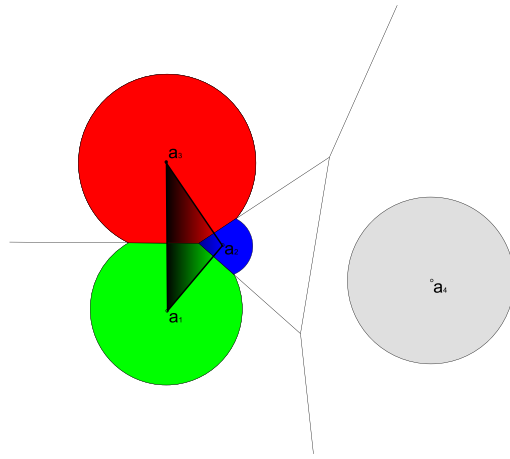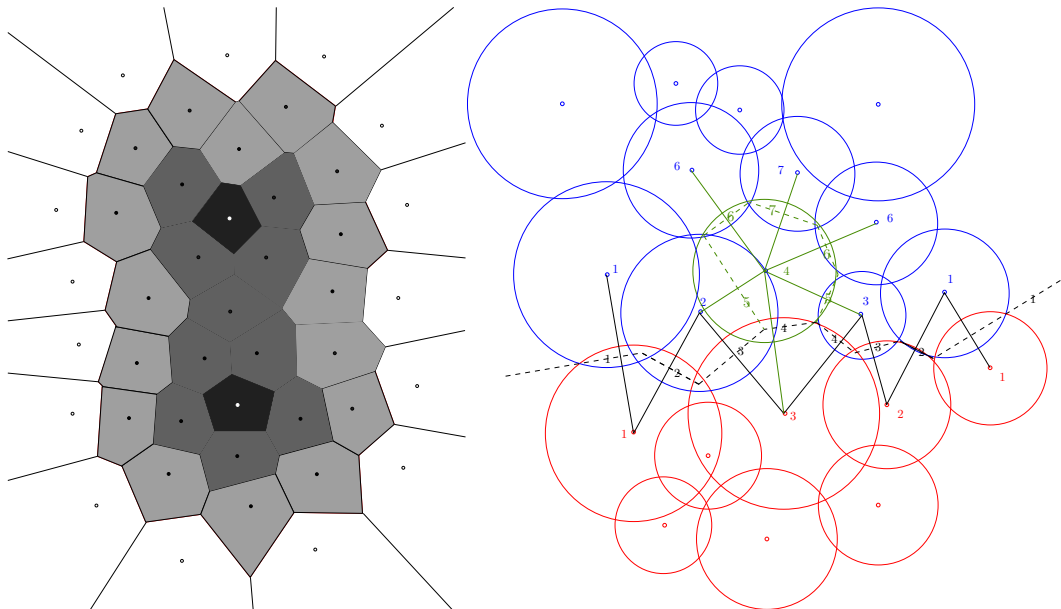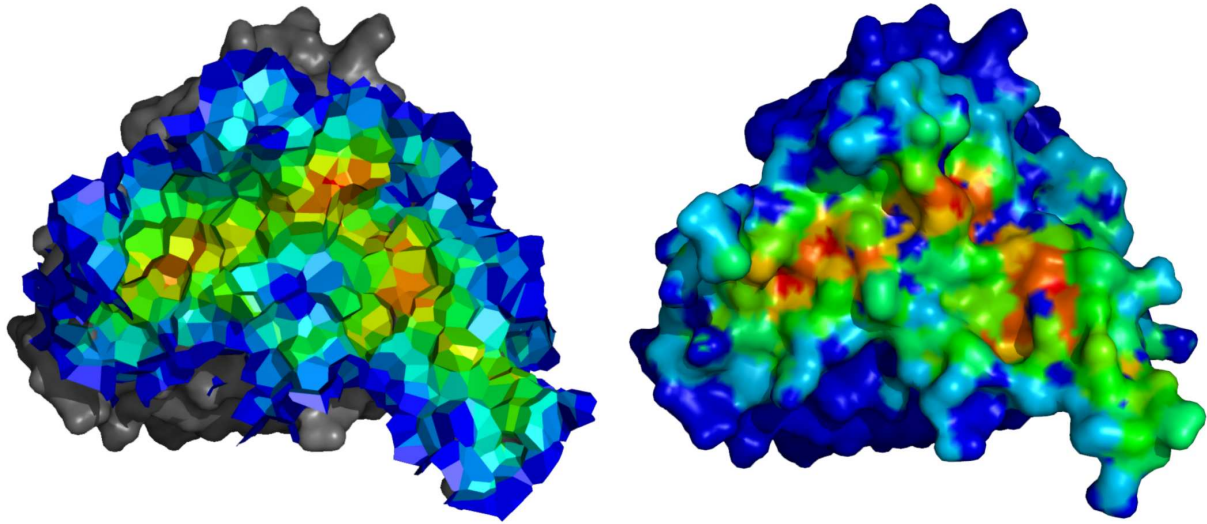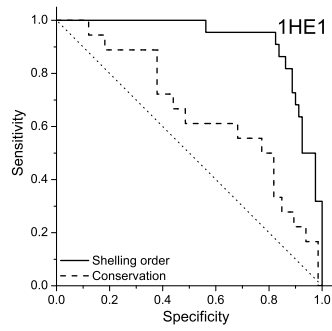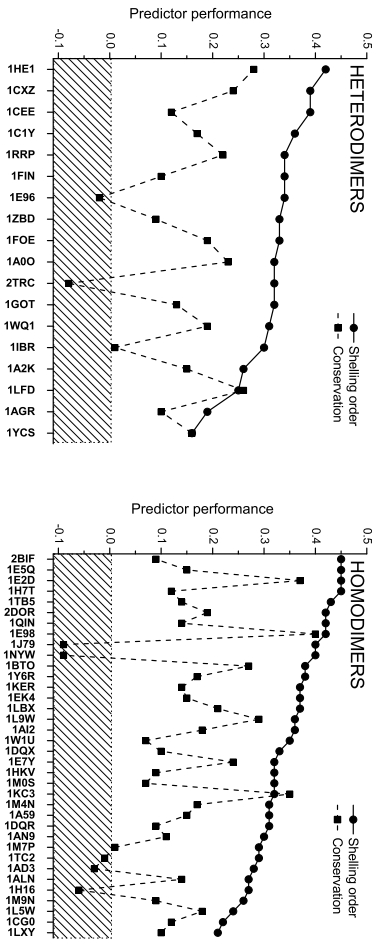
8 FIGURES

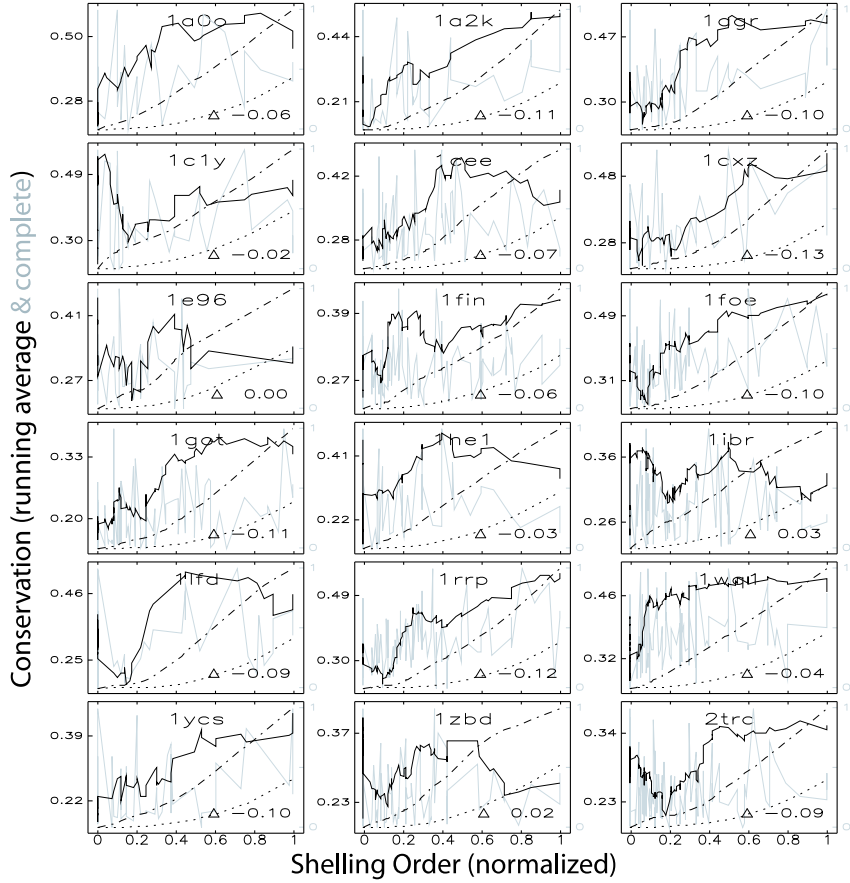Fig. 1.

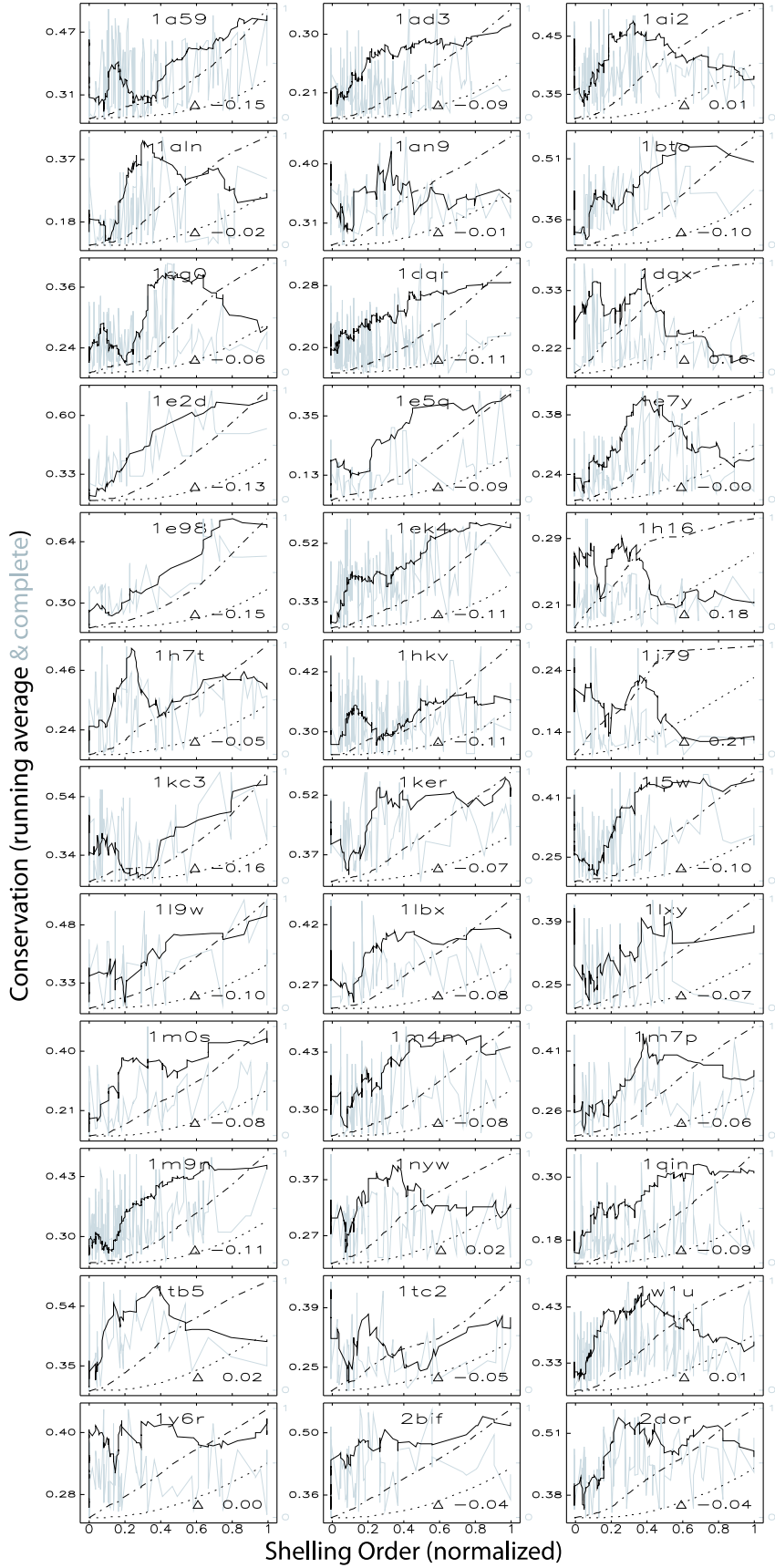Fig. 2. (a) and(b)

42

Fig. 3. (a) and(b)

Fig. 4.

43

Fig. 5.
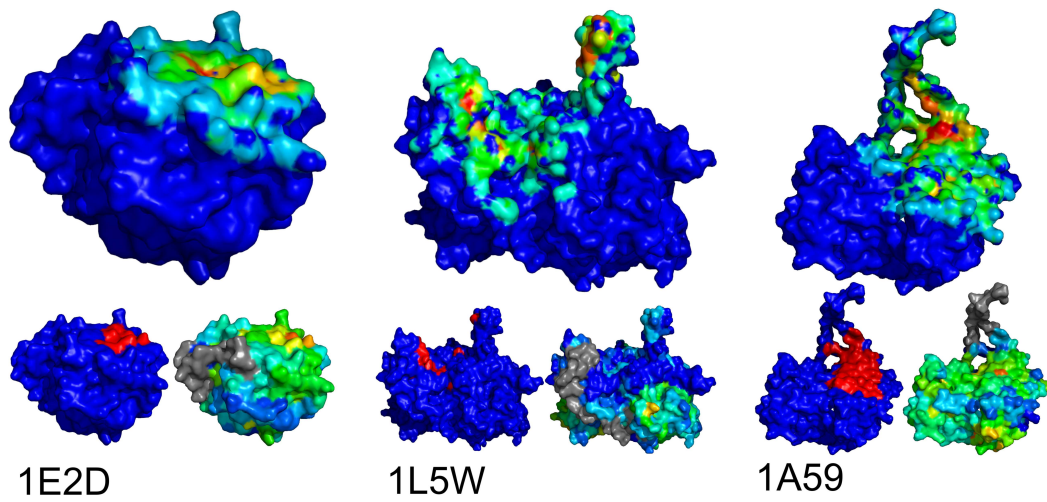
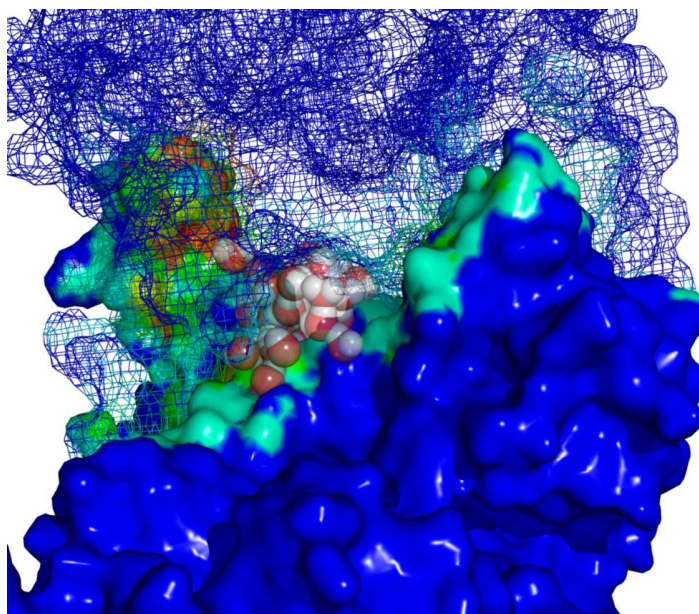Fig. 6.

Fig. 7.

1E2D   1L5W   1A59

Fig. 8.

Fig. 9.

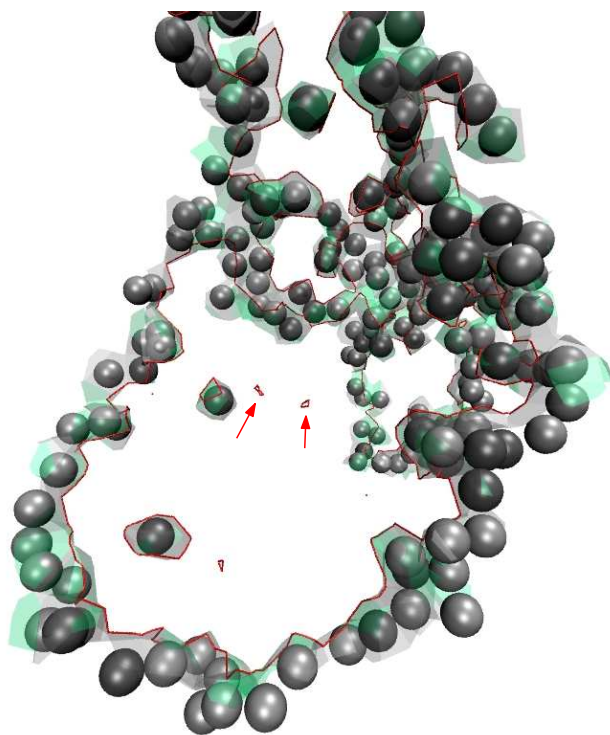Fig. 10.

A Supplemental Material

A.1 *Distribution of conserved residues: interface residues versus dry residues*

As outlined in section 3.2, we compare the spatial distribution of conservation in the entire set of interface residues with that of the dry residues.

We first consider all interface residues. To study the cumulated conservation score over consecutive shells, we compute the proportion of the interface conservation score which is contained in the subset of residues whose average VSO is lower than some value. Normalizing over shelling orders and varying the threshold yields a curve that rises from $(0, 0)$ (no residues selected, zero cumulative conservation) to $(1, 1)$ (all residues selected, 100% cumulative conservation). The area under this curve provides information about the variation of conservation with shelling order, since numerous highly conserved residues with low (high) shelling order will cause the curve to rise early (late) and result in large (small) areas.

Next, we focus on the dry residues and construct references with which to compare the previously computed areas, that quantify the relevance of rim residue conservation in each case. Denoting n_{dry} the number of dry residues of a given complex as reported in [26], we sort the interface residues by decreasing shelling order and assume the first n_{dry} only to be conserved –those with highest shelling orders. Let m and M be the minimum and maximum shelling orders in this subset, respectively (note that M is also the highest VSO found in the entire complex), and let $x = m/M$. The step function which is null from 0 to x, and equal to 1 from x to 1, maximizes the area $1 - x$ under the curve

49

₈₆₅ relative to the conservation of the subset of n_{dry} residues.

₈₆₆ As seen from Figure A.1, the rim residues account for a non-negligible part

₈₆₇ of the conservation: the area under the corresponding curve was found to be

₈₆₈ greater than the reference in all but two homodimer complexes, for which

₈₆₉ both measures were roughly equal. This could, in part, be due to a purely

₈₇₀ statistical effect: a large number of moderately conserved rim residues might

₈₇₁ end up having more weight than a small number of highly conserved core

₈₇₂ amino-acids. However, the peak in average conservation observed at the rim

₈₇₃ of many complexes (Section 3.2 (i)) proves that highly conserved residues

₈₇₄ occur on a non fortuitous basis at the rim of protein-protein interfaces – most

₈₇₅ likely as anchors for important electrostatic interactions that dictate complex

₈₇₆ formation and activity.

₈₇₇ *A.2   Validation of the sample preparation procedure*

₈₇₈ The procedure employed for the rehydration and equilibration of each of the

₈₇₉ complexes (Section 5) has deliberately been kept short, and can be run in

₈₈₀ minutes on a desktop computer. In this paragraph, we ascertain whether the

₈₈₁ placement and equilibration of the water molecules added using this fast pro-

₈₈₂ tocol are of sufficient quality for the current application. Of particular interest

₈₈₃ are the interfacial water molecules. When in simultaneous contact with both

₈₈₄ protein partners, they form the $AW - BW$ interface (Figure 2b and 10); but

₈₈₅ several layers of water inside a larger pocket will create holes in the interface,

₈₈₆ possibly splitting it into several connected components. The implications for

₈₈₇ shelling orders are crucial: in the first case, the water molecules will not af-

₈₈₈ fect the SO, while in the second scenario a boundary is created and the SO

50

889 consequently reset to 1.

890 The complex 1M0S, which features a large pocket filled with crystal water
891 molecules, was used for the test. A rigorous equilibration procedure, retaining
892 the crystal water molecules and involving a 5 ns molecular dynamics simulation
893 with state-of-the-art algorithms and parameters (Section 5), provided us with
894 a reference structure. Both this structure and the one from the fast procedure
895 were used as input to Intervor. Figure A.2 shows the tessellation of the AB
896 interface and the interfacial water molecules for both cases. Due to minor
897 conformational transitions that have occurred during the 5 ns MD simulation,
898 the two interfaces are not superposable. However, they retain the same shape
899 and number of connected components. In both cases, the central cavity is filled
900 with interfacial water that participates to the ABW interface. Both interfaces
901 feature boundaries of comparable lengths and topologies.

902 This difficult test case provides justification for our sample preparation method-
903 ology. It also represents a tribute to the robustness of our model, which de-
904 livers stable results upon variation of the solvation of the complex within a
905 reasonable range.

51

A.3 Figure legends

Legend of Fig. A.1. Area under the normalized cumulative conservation vs. shelling order curve (circles, solid line) and reference area (squares, dashed line), for all studied heterodimer (left panel) and homodimer (right panel) complexes – see text for details. Areas larger than the reference denote complexes for which rim residues are significantly conserved.

Legend of Fig. A.2. The AB interface (colored Voronoi facets) and the interfacial water molecules W (grey spheres) for two distinct rehydration and equilibration procedures – a fast (a) and a more exhaustive one (b); see text for details. Boundaries of the AB and $AW - BW$ interfaces are shown as red and green sticks, respectively.

PDB Id.	Proportion of conservation score for noninterface residues	Area under curve, interface residues	Reference
1YCS	0.76	0.57	0.53
1RRP	0.61	0.66	0.57
1E96	0.83	0.65	0.52
1CXZ	0.78	0.61	0.52
1LFD	0.80	0.51	0.16
1WQ1	0.64	0.67	0.66
1FOE	0.77	0.68	0.67
1AGR	0.77	0.64	0.64
1IBR	0.77	0.70	0.66
1FIN	0.75	0.61	0.59
1HE1	0.61	0.70	0.60
1A2K	0.70	0.71	0.66
1A0O	0.71	0.64	0.48
1ZBD	0.79	0.72	0.66
1GOT	0.83	0.60	0.51
2TRC	0.71	0.71	0.66
1CEE	0.62	0.61	0.42
1C1Y	0.77	0.66	0.47

Table A.1

Relationship of shelling order and conservation for the heterodimer set: proportion of total conservation provided by noninterface residues, area under the normalized cumulative conservation vs. VSO curve (see text), area under the corresponding 'reference' curve (see text).

PDB Id.	Proportion of conservation score for noninterface residues	Area under curve, interface residues	Reference
1A59	0.72	0.63	0.60
1H16	0.89	0.70	0.60
1M0S	0.73	0.49	0.42
1E5Q	0.97	0.55	0.32
1H7T	0.83	0.59	0.32
1E7Y	0.86	0.62	0.53
1ALN	0.64	0.60	0.62
1CG0	0.71	0.66	0.66
1E2D	0.81	0.64	0.55
1W1U	0.84	0.66	0.62
1KER	0.86	0.59	0.55
1EK4	0.74	0.63	0.64
1BTO	0.74	0.70	0.56
1QIN	0.36	0.62	0.45
1TB5	0.84	0.62	0.43
1M4N	0.76	0.64	0.52
2BIF	0.86	0.65	0.56
1M9N	0.57	0.70	0.68
1M7P	0.74	0.62	0.51
1E98	0.83	0.55	0.49
1L5W	0.95	0.70	0.62
1AD3	0.74	0.68	0.65
1J79	0.85	0.69	0.47
1AI2	0.62	0.68	0.61
1L9W	0.90	0.58	0.53
1LXY	0.87	0.66	0.51
1NYW	0.64	0.65	0.52
1KC3	0.87	0.66	0.58
1Y6R	0.72	0.68	0.66
1LBX	0.76	0.65	0.26
2DOR	0.72	0.59	0.43
1DQR	0.64	0.67	0.62
1AN9	0.85	0.64	0.56
1TC2	0.79	0.67	0.61
1HKV	0.72	0.63	0.54
1DQX	0.57	0.62	0.45

Table A.2

Relationship of shelling order and conservation for the homodimer set: proportion of total conservation provided by noninterface residues, area under the normalized cumulative conservation vs. VSO curve (see text), area under the corresponding 'reference' curve (see text).
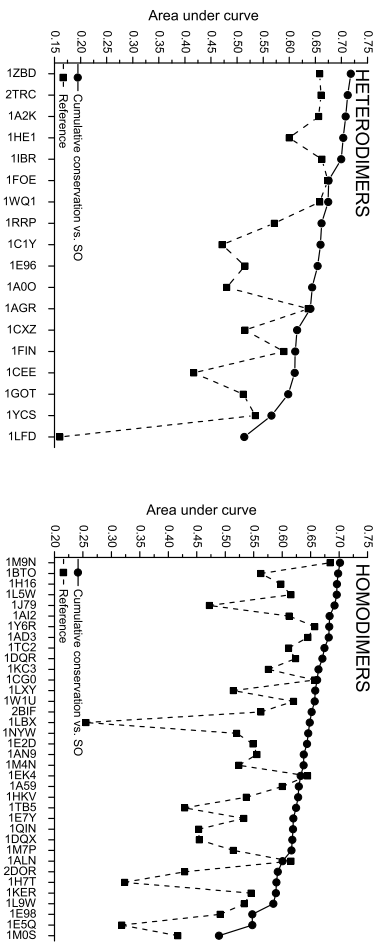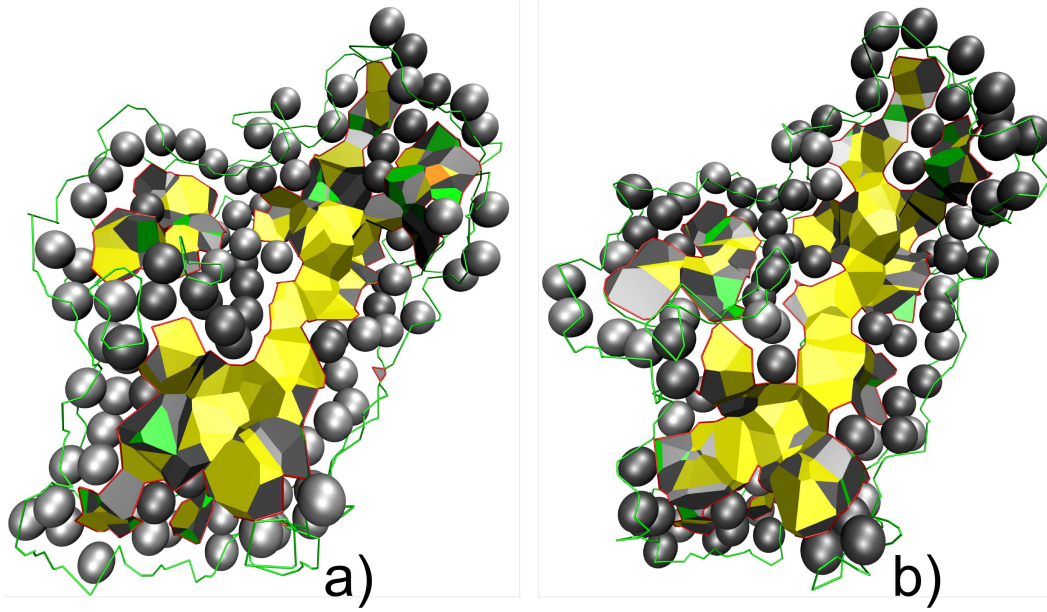
Fig. A.1.

Fig. A.2.